공학석사학위논문

지능형 연성 복합재 구동기를 이용한 모핑플랩 개발

Development of a Morphing Flap Using a Smart Soft Composite Actuator

2017년 2월

서울대학교 대학원

기계항공공학부

김 남 극

Abstract

Development of a Morphing Flap Using a Smart Soft Composite Actuator

Nam-Geuk Kim
Department of Mechanical and Aerospace Engineering
The Graduate School
Seoul National University

A morphing flap can change the trailing edge of a wing and act like a flap. The advantage of a morphing flap is that it can maintain the continuous surface profile of a wing, which can reduce turbulence, aerodynamic drag, vibration, and noise, versus the discontinuous geometry of 'conventional' flaps and wings. The morphing technology, using smart materials, can be applied in various fields, such as biomimetic robots and aviation, Since it can achieve various deformations without complex mechanical components, such as motors and joints. These morphing technologies are advantageous to reduce the operating cost of the aircraft through weight saving. In this study, we designed and fabricated a smart soft composite (SSC) actuator, integrated with a shape memory polymer (SMP) scaffold and a shape memory alloy (SMA) wire. The fabricated SMP-SMA based SSC actuator can maintain a deformed state without additional current to heat the SMA. The measured maximum deformation angle of the actuator was 102° and the maintained angle was 70°. A morphing flap was then designed and fabricated using the SMP-SMA based SSC actuator. The aerodynamic performance of the morphing

flap was evaluated in wind-tunnel experiments. The morphing flap generated additional lift force during actuation and the lift to drag ratio of the morphing flap was higher than that of a conventional flap; the maximum difference was 81% at 10°.

Keyword : Smart materials; Morphing structure; Morphing flaps ; Smart soft composite (SSC).

Student Number : 2015-20711

Contents

Chapter 1. Introduction 1

1.1 Overview 1

1.2 Morphing wing 5

1.3 Smart Soft Composite actuator 7

1.4 Purpose of research 8

Chapter 2. Materials 9

2.1 Shape Memory Alloy 9

2.2 Shape Memory Polymer 11

2.3 PDMS and Ecoflex 13

Chapter 3. Design 14

3.1 SMA-SMP based SSC actuator 14

3.2 Morphing flap 18

Chapter 4. Maufacturing 24

4.1 SMA-SMP based SSC actuator 24

4.2 Morphing flap 27

Chapter 5. Experiment and result 30

5.1 SMP-SMA based SSC actuator performance evaluation 30

5.2 Morphing flap performance evaluation 34

Chapter 6. Conclusion 43

Reference 44

Abstract in Korean 48

List of Figures

Figure 1.1 Wing and flap of commercial airliner 2

Figure 1.2 Flow analysis result of conventional flap and morphing flap 6

Figure 2.1 Schematic image of phase change of the shape memory alloy 9

Figure 2.2 The recovery force of shape memory polymer beam 10

Figure 3.1 Schematic diagram of the mechanism of the SMA wire-based smart soft composite (SSC) actuator. 10

Figure 3.2 Schematic design of the SMP-SMA-based SSC actuator..... 17

Figure 3.3 The schematic image of morphing flap and wind segment 18

Figure 3.4 Finite element analysis results regarding surface deformation when the top and bottom surfaces were made of polydimethylsiloxane (PDMS) 19

Figure 3.5 Variation in deformation depending on surface configuration 20

Figure 3.6 Pressure distribution over the morphing flap and wing.... 21

Figure 3.7 Design of flexible structure using thermoplastic polyurethane (TPU) 22

Figure 3.8 Design of the morphing flap 23

Figure 4.1 Fabrication process for the SMP-SMA based SSC actuator. 25

Figure 4.2 Schematic layout of SMP-SMA based composite SSC actuator and fabricated specimen.. 26

Figure 4.3 The fabrication process for the morphing flap..... 28

Figure 4.4 Fabricated morphing flap..... 29

Figure 4.5 Fabricated wing segment with morphing flap..... 29

Figure 5.1 Actuator performance experiments set up 30

Figure 5.2 Time-series thermal images of SMP-SMA based actuator surface when each components are heated and cooled.. 31

Figure 5.3 Activation sequence, temperature changes, and deformation of SMP and SMA of the SSC. 33

Figure 5.4 Deformation of morphing flap..... 35

Figure 5.5 Schematic image of wind tunnel experimental set-up..... 36

Figure 5.6 The morphing flap and conventional flap experiment set-up 36

Figure 5.7 Changes in lift forces depend on morphing flap actuation (AOA : 2°)..... 39

Figure 5.8 The morphing Aerodynamic coefficient of actuated and un-actuated morphing flap as a function of the angle of attack..... 40~41

Figure 5.9 Lift to drag ratio of the morphing flap and the conventional flap as a function of the angle of attack 42

List of Tables

Table 2.1 Material properties of the shape memory alloy (SMA) 10

Table 2.2 Mechanical properties of the shape memory polymer (SMP). 12

Table 2.3 Mechanical properties of polydimethylsiloxane (PDMS) .. 13

Table 3.1 Mechanical properties of thermoplastic polyurethane (TPU) 22

Chapter 1. Introduction

1.1 Overview

The geometry of a wing is one factor that affects the aerodynamic performance of airplanes. A fixed-wing geometry is not effective given the variety of flight environments, such as cruising, take-off, and landing [1]. Birds optimize flight efficiency by changing their wings to an optimal shape for each situation, such as cruising, hunting, surveillance, and observation. Consequently, in modern aircraft, variety devices, such as slats, flaps, and sweep angle-changing devices, have been developed to modify the wing shape in various flight situations [2]. In this way, the 'conventional' flaps of commercial airliners or unmanned aerial vehicles (UAVs) have additional components installed in their wing that are used to generate additional lift when required as shown in figure 1.1 [3].

However, additional mechanical components, such as hydraulic actuators and motors, to operate and mount these devices, lead to increased weight, which is directly linked to increased costs associated with aircraft operations [4, 5].

Devices such as flaps operate with mechanical components and mechanisms; there is a discontinuity between the wing and the flap surface. Turbulence is generated at these discontinuous surfaces, which not only degrades the aerodynamic efficiency of the entire wing but also acts as a major source of noise, vibration, and drag [6, 7].

Figure 1.1 Wing and flap of commercial airliner (A380)

Recently, unmanned airplanes have been used for various purposes, including vaccine delivery, surveillance, and reconnaissance, and demand for them is increasing rapidly[8-10]. Extending the time and distance of missions is an important issue in the operation of such UAVs [11]. Research on increasing the efficiency of wings has been conducted and studies on wings having continuous wing surfaces have been active since the early 2000s[12, 13].

Morphing wings are divided into two categories: (1) platform alterations and (2) airfoil profile and camber adjustments[2, 14]. Platform alterations refer to those measures that change the span area, chord length, and sweep angle of the wing. As examples, Blondeau et al. proposed a mechanism for resizing the span of a wing structure using a pneumatic actuator [15], and Yu et al. used shape memory polymer (SMP) to change the sweep angle of a wing [16]. Hugo et al. designed a twisting wing using a shape memory alloy (SMA) wire-based smart soft composite (SSC) actuator [17]. Han et al. developed a morphing winglet actuated by a SMA fiber/woven composite actuator that could reduce the induced drag [18].

Airfoil profile and camber adjustments refer to changing the shape of the airfoil using a conventional actuator in the wing or a smart material, such as SMA or lead zirconite titanate (PZT). Strelec et al. designed and fabricated a morphing wing using SMA wire[19]. Pinkerton et al. proposed a PZT composite-based morphing airfoil [20]. Other methods for deforming wings include using 'conventional' mechanical parts, such as linear actuators and servo motors[21-24].

This study focused on designing and fabricating a morphing flap using a SMP-SMA-based SSC actuator and evaluating the aerodynamic performance of the morphing flap. The SMP-SMA based SSC actuator consisted of a SMP and SMA, a PVC scaffold, and a polydimethylsiloxane (PDMS) matrix. A morphing flap was fabricated using the SMP-SMA based SSC actuator and implemented on the wing structure of a UAV wing to measure aerodynamic performance. The aerodynamic performance and structural stability of the morphing flap in a flight environment was tested by wind-tunnel experiments.

1.2 Morphing wing

The aerodynamic characteristics of the wing are greatly influenced by the shape of the wing. Many devices have been developed to change the wings during flight in order to achieve appropriate efficiency in various flight environments. Flaps have also been developed as devices for generating additional lift, and there are various types of flaps to increase their efficiency. However, existing devices such as flaps have a discontinuous shape with the wing, which adds additional factors that degrade aerodynamic efficiency, such as drag and vibration. Therefore, research is underway on adaptive wing or compliant wing in which the wing itself deforms instead of an additional device such as a separate flap.

The morphing flap can be seen as one of adaptive wing or compliant wing concept and it changes the trailing edge of the wing so that it can act as a flap. Figure 1.2 shows the results of flow analysis of conventional plain flap and morphing flap. As can be seen from the results, the turbulence occurs in the discontinuous gap between the flap and the wing of the conventional flap. Also, the lift to drag ratio of the morphing flap is about 41.3% higher than that of the conventional flap.

The small efficiency differences in the wing cause significant differences in aircraft operating costs such as fuel consumption. Furthermore, increasing the efficiency of the wing is one of the big issues for UAVs and transportation planes that have to be bloomed for a long time.

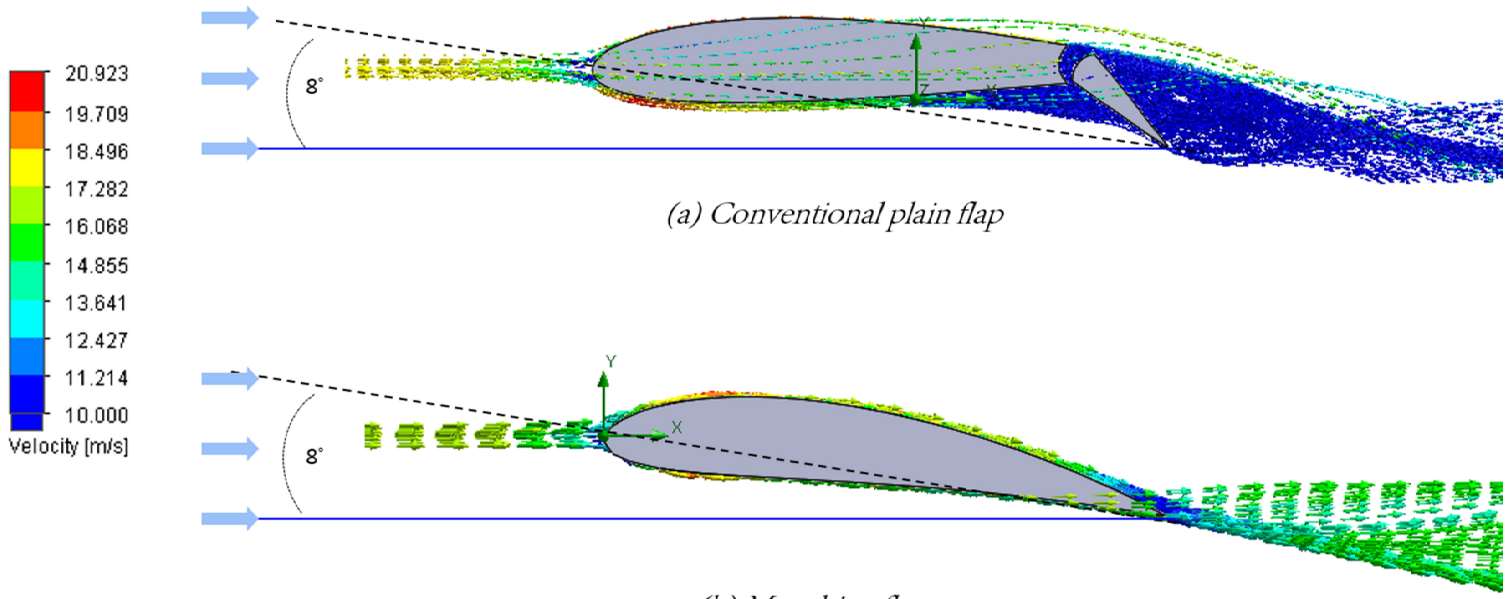

Figure 1.2 Flow analysis result of conventional flap and morphing flap

1.3. Smart Soft Composite Actuator

Smart Soft Composite (SSC) Actuator refers to a composite actuator that has the desired driving characteristics by placing smart materials such as SMAs, SMP, and IPMC inside a layered composite [25, 26].

The basic structure of the SSC actuator is composed of a smart material as a driving source, a scaffold as a rigid support that maintains the rigidity of the actuator, determines the driving characteristics, and a polymer matrix that combines all the components into one structure. Each of the components is arranged in the form of a layer inside the SSC actuator [27].

The driving characteristics of the SSC actuator depend on the arrangement of the driving source such as SMAs and the scaffold design of the rigid support on the neutral surface of all actuators. The characteristics of these SSC actuators are that they can be implemented without mechanical components such as hinges, joints, and motors. Therefore, the SSC actuator has advantages as a lightweight driving source [28].

The SSC actuator can be freely modified as well as the shape of the polymer matrix, as well as the layout of the smart material used as the drive source and the design of the scaffold. Because of this characteristic, SSC actuator can be easily applied to various fields.

1.4. Purpose of research

In this study, we aimed to develop a morphing flap with wings and continuous surface shapes using SMAs and SMPs based SSC actuators. In order to achieve these research goals, we divided into two subcategories of SMP-SMA based SSC actuator development and morphing flap development.

In the development of SMP-SMA based SSC actuators, the use of SMP to improve energy efficiency, which is considered as a disadvantage of conventional SMA-based SSC actuators and the design of the SMP scaffold and the operating sequences of all actuators were optimized. We also aimed to evaluate the performance of the fabricated actuator and to find the optimal design conditions for the application to the morphing flap.

We will also test the manufactured morphing flap in wind tunnel to evaluate aerodynamic performance such as lift to drag ratio. In addition, the conventional flap is additionally tested to confirm whether the aerodynamic performance of the morphing flap is improved.

Chapter 2. Materials

2.1 Shape Memory Alloy

In 1932, silver and cadmium−based shape memory effects were first discovered, but NiTi based SMAs with remarkable strain were developed in 1971 [29, 30].

Widely used SMAs that demonstrate the shape memory effect (SME) [24] include Ni− and Ti−based SMAs was developed by US navy ordnance laboratories in 1971. As the temperature changes, the phase of the SMA changes, from an austenite to a martensite phase. During such phase changes, SMA changes its shape to its original shape as shown is figure 2.1.

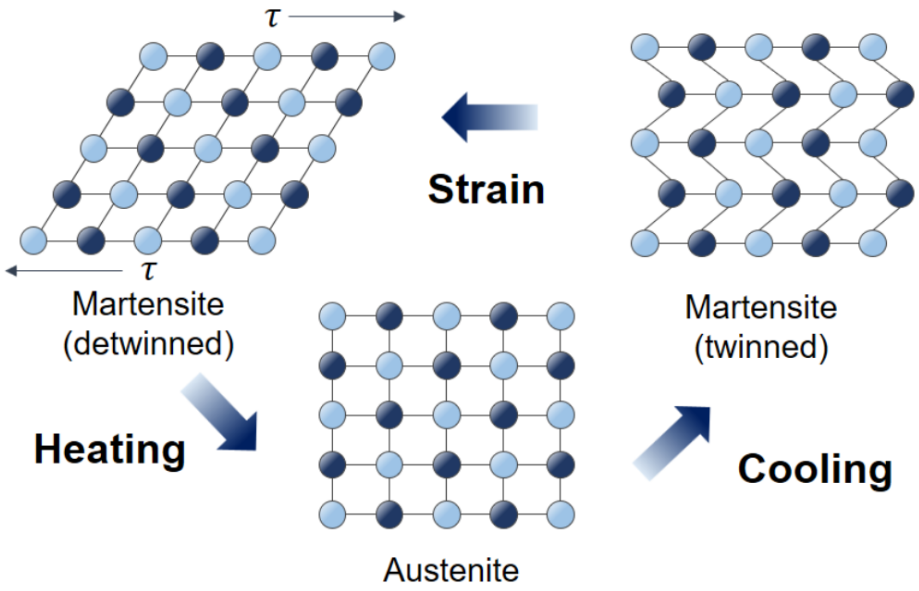

Figure 2.1 Schematic image of phase change of the shape memory alloy

The transition temperature varies, depending on the composition ratio of Ni and Ti in the SMA [26]. SMAs have advantages over other shape memory materials, such as their shape memory ability, processability, and mechanical properties. The mechanical properties of SMAs are shown in Table 2.1.

SMAs can be processed into various forms, such as films, tubes, rods, and wires. SMAs are being used in various applications, such as in new drive sources to replace traditional ones, such as a motor or hydraulic system [31]. SMA wires show linear deformation, but can also show complex deformations when used in a structural design with twisting and bending [25, 27, 32–35].

Table 2.1 Material properties of the shape memory alloy (SMA).

Parameter	Description	Value
Young's modulus	Austenite (E_A)	75 GPa
	Martensite (E_M)	28 GPa
Phase transformation temperature	Austenite start (T_{As})	68℃
	Austenite finish (T_{Af})	78℃
	Martensite start ($T_{M\,s}$)	52℃
	Martensite finish ($T_{M\,f}$)	42℃
Specific heat capacity	C	0.322 J/g℃
Maximum deformation ratio	$\varepsilon_{m\,ax}$	8%

2.2 Shape Memory Polymer

SMPs also have shape memory properties. There are several ways of inducing SMEs in SMPs, such as light (UV, IR), temperature, and magnetic fields [36].

SMPs has the advantage that it can be processed into a desired shape more easily than a material such as a metal or an alloy due to the characteristics of the material itself [37]. It is light and easy to deform as compared with SMA, and it has a large recovery strain.

The temperature-induced SMP is in a rubbery state at high temperature and a glassy state at lower temperature. Due to the lower modulus in the rubbery state, the material can be deformed its shape by an external force and the SMPs stores elastic stress during such deformation. However, such stress is not sufficient to recover the original shape in the glassy state as shown in figure 2.2. The SMP in a glassy state has a higher modulus than the rubbery state [36, 38](Table 2.2). Thus, many studies have attempted to use the stiffness change characteristics of SMPs to deform the shape of a robot or structure and to maintain a deformed state[39]. Similarly, our research used a SMP as a stiffening control material for SSC actuator.

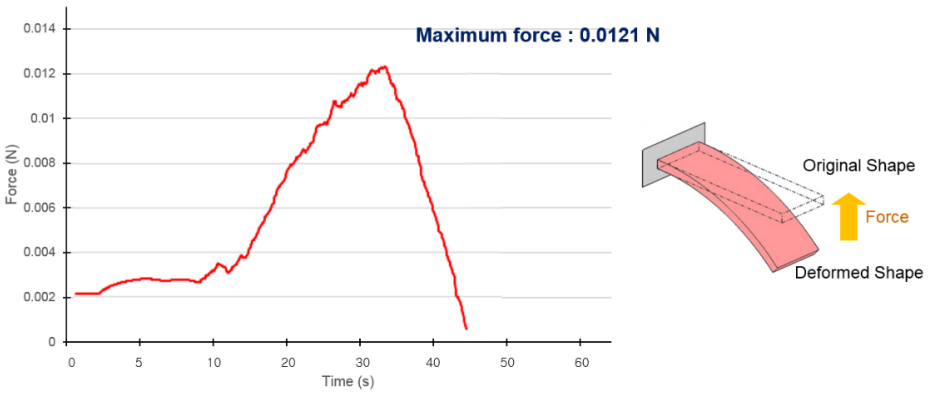

Figure 2.2 The recovery force of shape memory polymer beam

Table 2.2 Mechanical properties of the shape memory polymer (SMP).

Parameter	Value	
	Glassy state	Rubbery state
100% modulus		2.1 MPa
Tensile strength	48 MPa	13 MPa
Elongation	30 ~ 50%	~ 600%
Bending modulus	2,150 MPa	
Bending strength	80 MPa	
Specific gravity	1.25	1.25
Glass transition temperature	55℃	

2.3 PDMS and Ecoflex (Matrix)

PDMS was used to integrate of the SSC actuator (the SMA and scaffold) into a single structure. PDMS in the SSC actuator acted as a matrix and elastomer, using the mechanical properties of PDMS as shown in the table 2.3. Due to the characteristics of PDMS, it has been used widely for various purposes, such as in biomedical systems and micro electro mechanical systems (MEMS) [40].

The ecoflex used in this study was Ecoflex 0030 manufactured by smooth-on. The ecoflex is an elastomeric rubber with a tensile strength of 1.37 MPa, which is 20% of PDMS.

The properties of polymers such as PDMS and Ecoflex are widely used in soft robotics such as underwater ray robots [41].

Table 2.3 Mechanical properties of polydimethylsiloxane (PDMS).

Parameter	Value
Young's modulus	1.84 MPa
Tensile strength	6.7 MPa
Specific gravity (cured)	1.03
Density	965 kg/m3

Chapter 3. Designs

3.1 SMA-SMP based SSC actuator

A SMP-SMA-based SSC actuator was proposed to actuate a morphing flap by inserting an actuating source within an integrated structure. Using this approach, lightweight wing structures can be achieved by replacing mechanical parts, such as conventional motors and hydraulic devices. The SSC actuator design consists of composite layers that provide an anisotropic material composition, including smart materials to provide a driving force for the actuator, such as SMAs and SMPs, in the polymer matrix. This SSC is layered with an PVC scaffold, SMA wire, and SMP scaffold. The ABS scaffold acts as a rigid support for the SSC actuator. The design of the scaffold determines the actuation characteristics of the actuator. Various actuation motions and mechanical properties can be controlled by appropriately designing the SSC composite.

Figure 3.1 is a simplified illustration of the operating principles of the SSC actuator. The SMA wire contracts on heating, causing deformation due to the eccentricity of the SMA at the center of the matrix. The positioning of the SMA wire can change the actuation characteristic; using this principle, complex actuation, such as bending or twisting can be achieved relatively simply, without complex components such as hinges or joints [25, 42]. Additionally, such structures can simulate complex motions, such as the fin motions of a turtle or stingray; as such, they have been used widely in biomimetic robots[41, 43]. There have also been various studies of aerodynamic structures using light and simple SSC mechanisms, such as a SSC-based winglet for UAVs and rear spoilers of vehicles [17, 44]

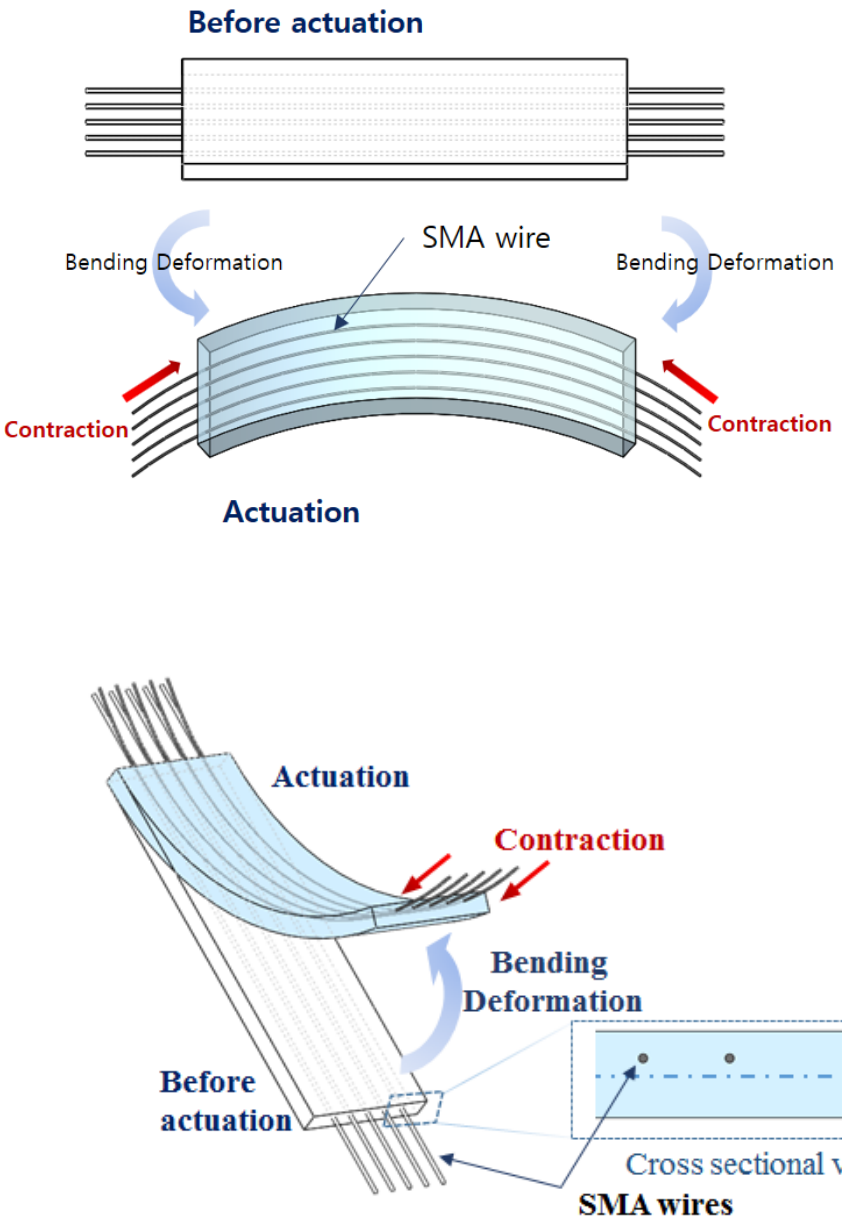

Figure 3.1 Schematic diagram of the mechanism of the SMA wire-based smart soft composite (SSC) actuator.

However, there is the limitation that SMA wires must be kept heated to maintain strain in a SSC actuator. This lowers the energy efficiency of structures and the system, as a whole, such as in airplane flaps and robot fingers that are required to maintain the deformed state for a certain period of time [44, 45]. The SMP has a lower modulus at the higher temperature and in its rubbery state; however, it maintains a high modulus in the glassy state, below the glass transition temperature (T_g). Given these characteristics, the SMP was inserted into the SSC actuator for the flap in the form of a scaffold. Figure 3.2 shows a schematic design of the SMP-SMA based SSC actuator; a nichrome wire was used to increase the temperature of the SMP and was inserted into a layer of the SSC actuator.

The SMP-SMA based SSC actuator has the advantage of higher energy efficiency than conventional SMA based actuators, because it is not necessary to heat the SMA to maintain the deformed state. During contraction of the SMA wires, the SMP is heated to decrease stiffness; when the structure is completely deformed, the SMP is cooled to keep the entire SSC structure in the deformed state.

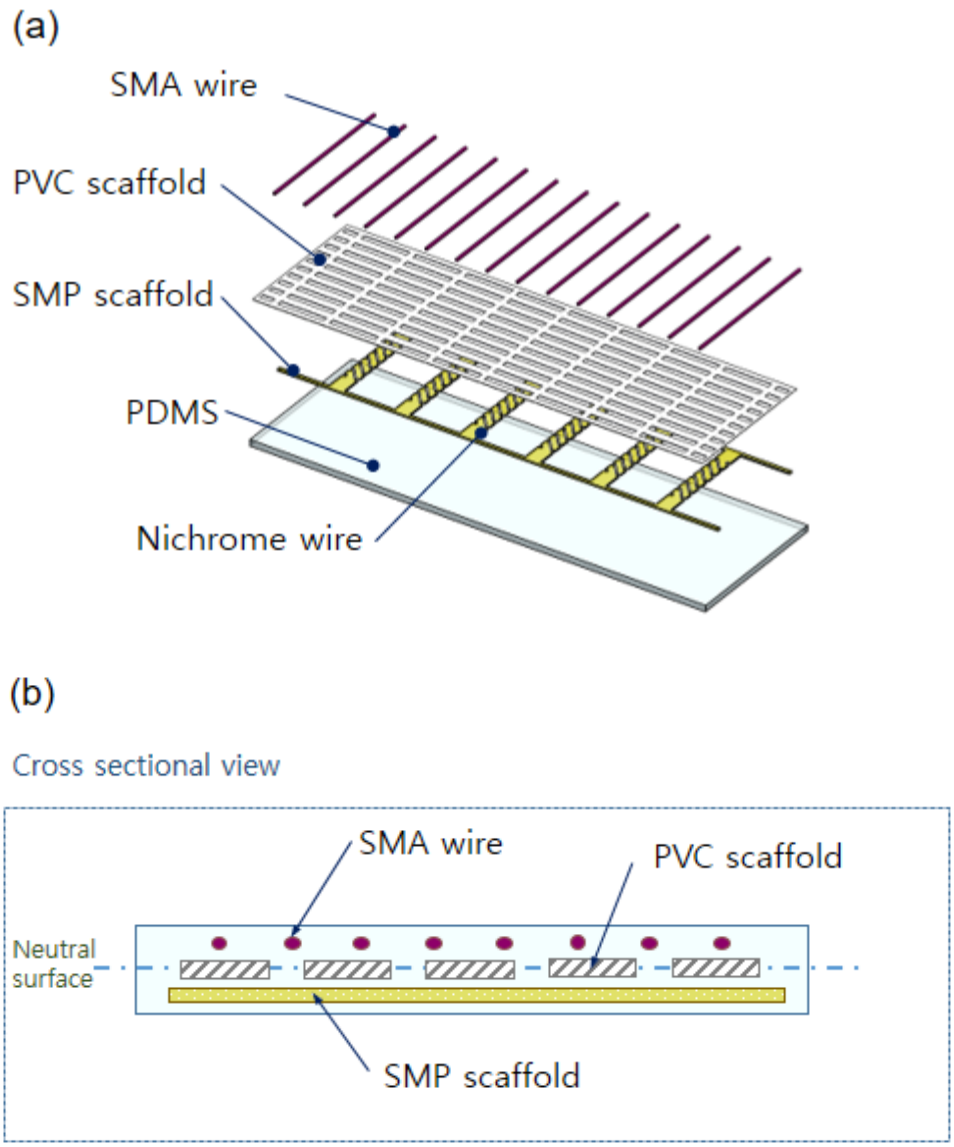

Figure 3.2 Schematic design of the SMP-SMA-based SSC actuator (a) isometric view and (b) cross-sectional view.

3.2 Morphing flap

A flap is a high lift device, mounted within the wing structure of an airplane. The flap is used to increase the lift of the wing at a given airspeed. When the flap is operated, the camber angle of the wing is increased, and thus the lift is increased, by increasing the angle of attack.

The basic concept of the morphing flap is to modify the chord line of the wing by deforming the trailing edge of the wing, and it is designed to be mounted as a module in the unmorphed wing segment of the wing as shown in figure 3.3. The morphing flap has the same curvature as the wing surface, so the entire wing, including the flap, has a continuous surface with actuation of the flap.

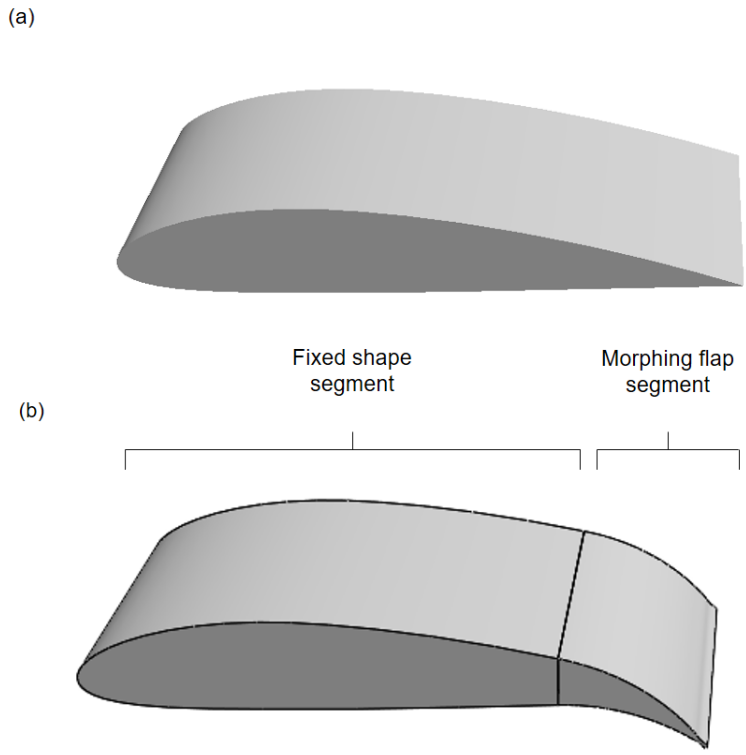

Figure 3.3. The schematic image of morphing flap and wind segment: (a) the original wing shape; (b) the fixed and morphing flap segment.

The design of the morphing flap is based on a bending actuator using a SMP–SMA system. The actuator is embedded within the integrated flap structure to actuate the morphing flap, as opposed to using mechanical components, such as a motor and hydraulic system.

The surface of the morphing flap must maintain a continuous curvature while the flap is actuated. When the flap is deformed, the sides of the flap surface have differing strains. According to finite element (FE) analysis of the deformation of the flap surface, the top surface of the flap required 6% more strain than the bottom surface to maintain the curvature of an air foil. Figure 3.4 shows the FE analysis of deformation during flap actuation with the SMA wire when the top and bottom surface are made of the same material, PDMS. Buckling and unexpected curvature occurred at the flap surface. To enhance the elasticity of the top surface, Ecoflex (00–30) and PDMS were combined in a square pattern to increase adhesion between the materials as shown in figure 3.5.

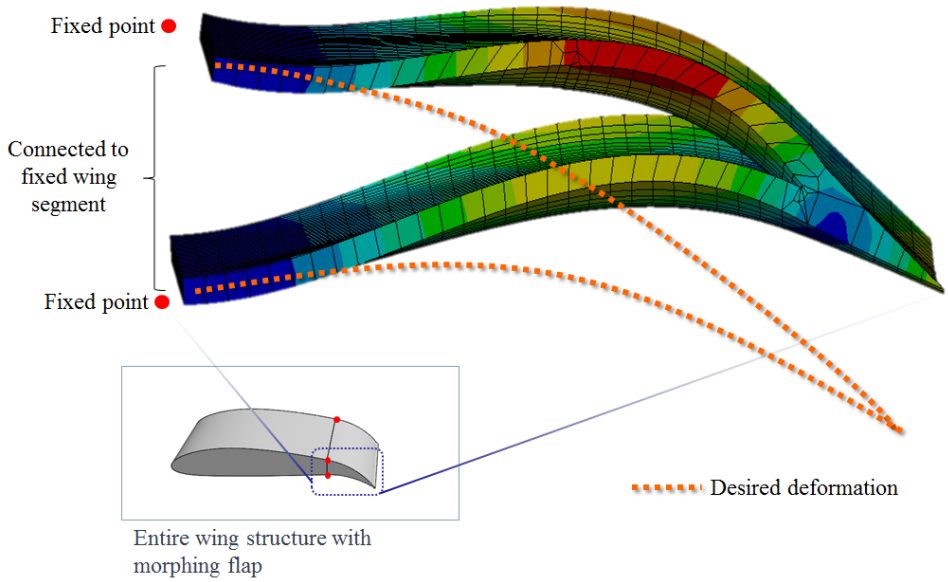

Figure 3.4 Finite element analysis results regarding surface deformation when the top and bottom surfaces were made of polydimethylsiloxane (PDMS).

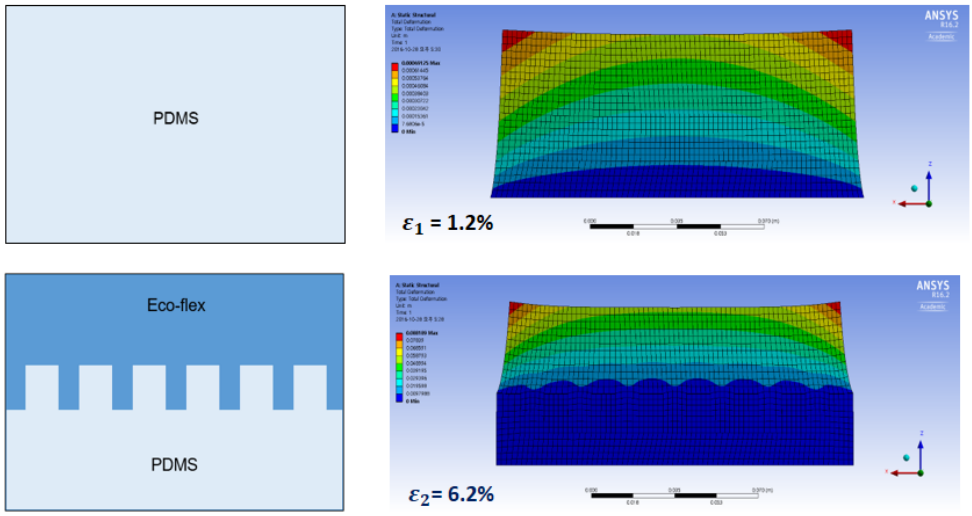

Figure 3.5 Variation in deformation depending on surface configuration

Aerodynamic forces are applied to the wing surface during flight as shown in figure 3.6; indeed, the pressure makes it difficult to maintain the curvature of the flexible flap. A 3D printed thermoplastic polyurethane (TPU) structure was inserted to maintain the shape of the entire flap during flight. The design of TPU is shown in figure 11.

The TPU used was a filament type, Ninjaflex (Ninjatek Inc.); the printed structure was also flexible and could be deformed under actuator operation as needed. Table 3.1 shows the mechanical properties of TPU.

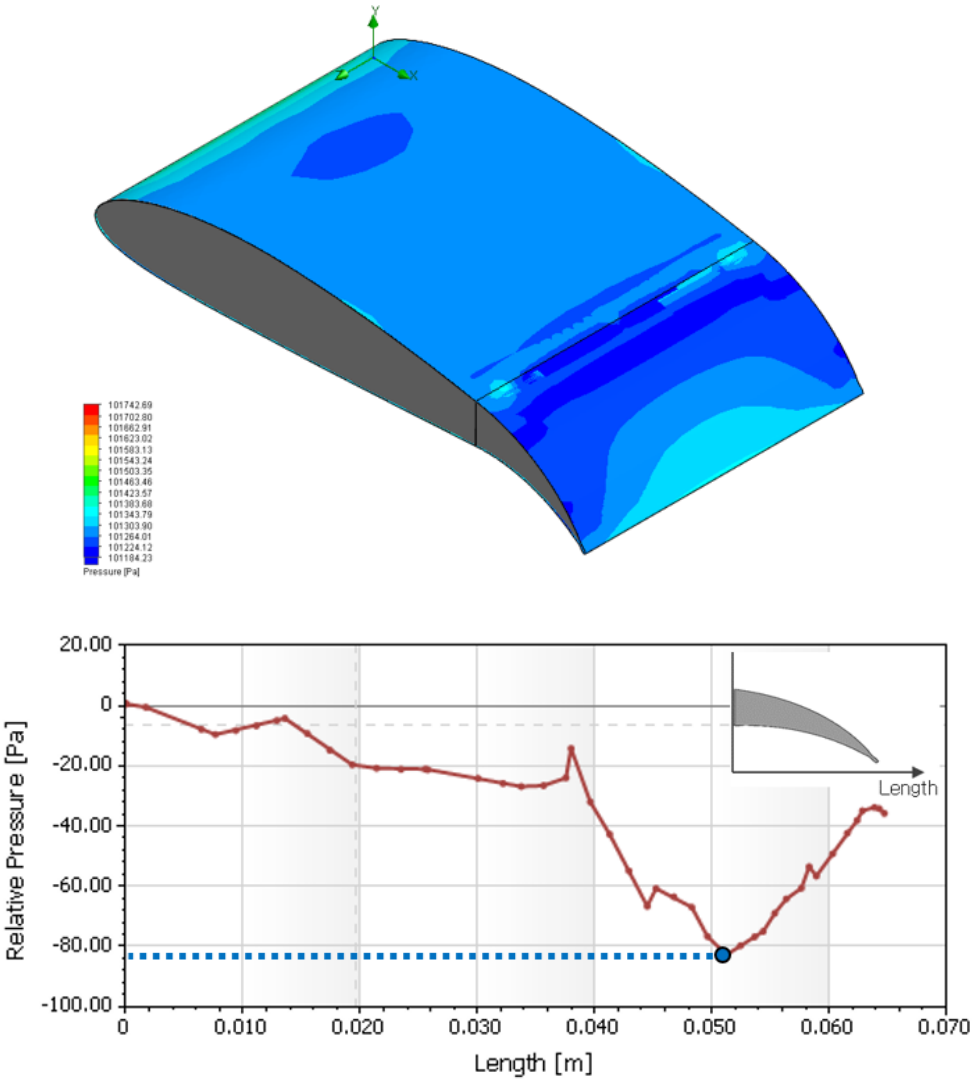

Figure 3.6 Pressure distribution over the morphing flap and wing

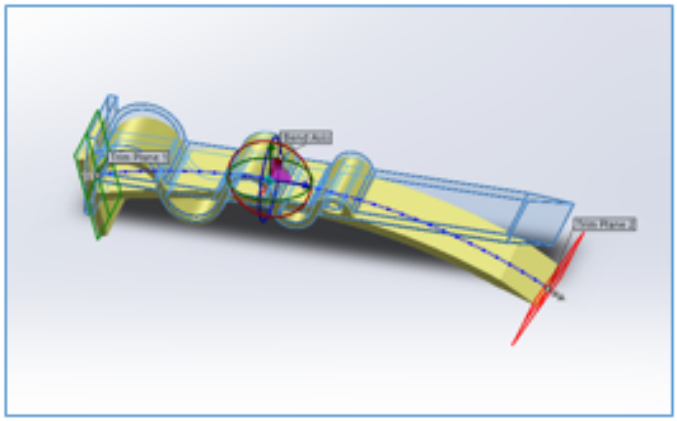

Figure 3.7 Design of flexible structure using thermoplastic polyurethane (TPU).

Table 3.1 Mechanical properties of thermoplastic polyurethane (TPU).

Parameter	Value
Tensile strength	3.99 MPa
Tensile modulus	12.41 MPa
Elongation at break	660 %
Elongation at yield	65%
Specific gravity	1.19

A prototype morphing flap was designed to have the same shape as the curvature of the entire airfoil at the rear of the wing; the SMP–SMA based composite actuator was embedded in the lower surface of the flap. Figure 3.8 shows a schematic design of the morphing flap prototype. The flexible structure was placed inside the internal space of the morphing flap. The span of the morphing flap was 150 mm, the width was 55 mm, and both sides of the flap were integrated together, within one structure.

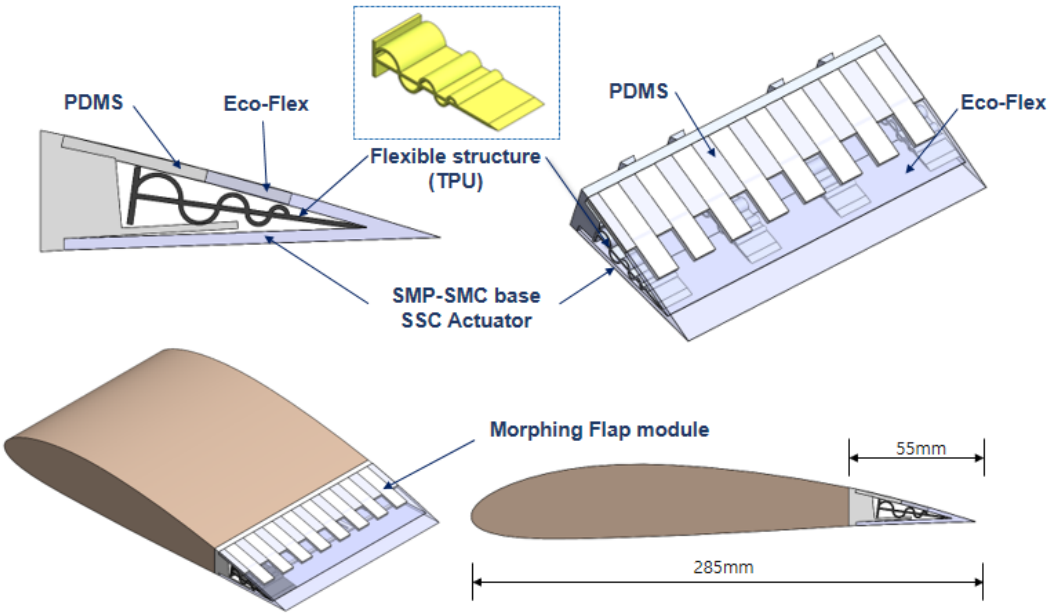

Figure 3.8 Design of the morphing flap.

Chapter 4. Manufacturing

4.1 SMP-SMA based SSC actuator

The SMP-SMA based SSC actuator was fabricated using molds, with SMA wire, polyvinyl chloride (PVC), a SMP scaffold, and a PDMS polymer matrix. The mold and SMP scaffold structure were fabricated by 'fused deposition manufacturing' (FDM) technology, using a three-dimensional (3D) printer.

The scaffold was processed by laser cutting of the PVC film. The surface of the SMP scaffold was wrapped with nichrome wire at certain intervals. Components of the SSC actuator were placed in a mold and PDMS polymer was injected using a syringe.

The PDMS used was Sylard 184 from Dow Corning, in a mixture with hardener at a 1:10 ratio. The SMA wire used was 0.25 ㎜ diameter Flexinol wire (nickel-titanium alloy actuator wire), manufactured by Dynalloy, Inc. (Irvine, CA, USA). The assembled components in the mold were then cured at 55℃ for 8 hours in an oven. The assembly and fabrication process for the SMP-SMA based SSC actuator is shown in figure 4.1, and the fabricated actuator is shown in figure 4.2.

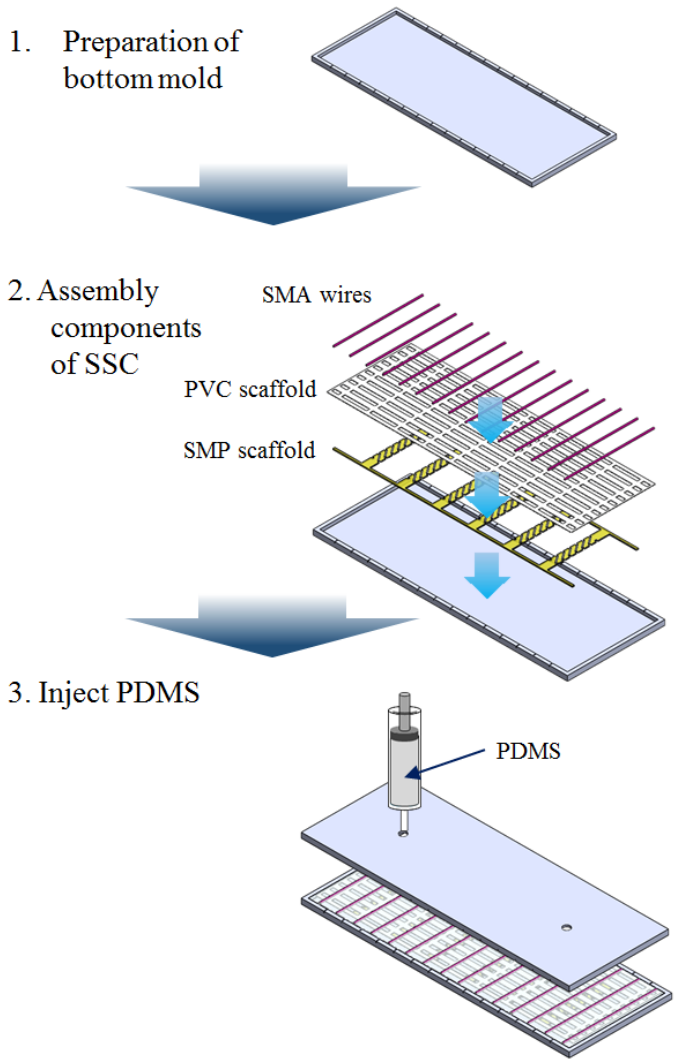

Figure 4.1. Fabrication process for the SMP-SMA based SSC actuator.

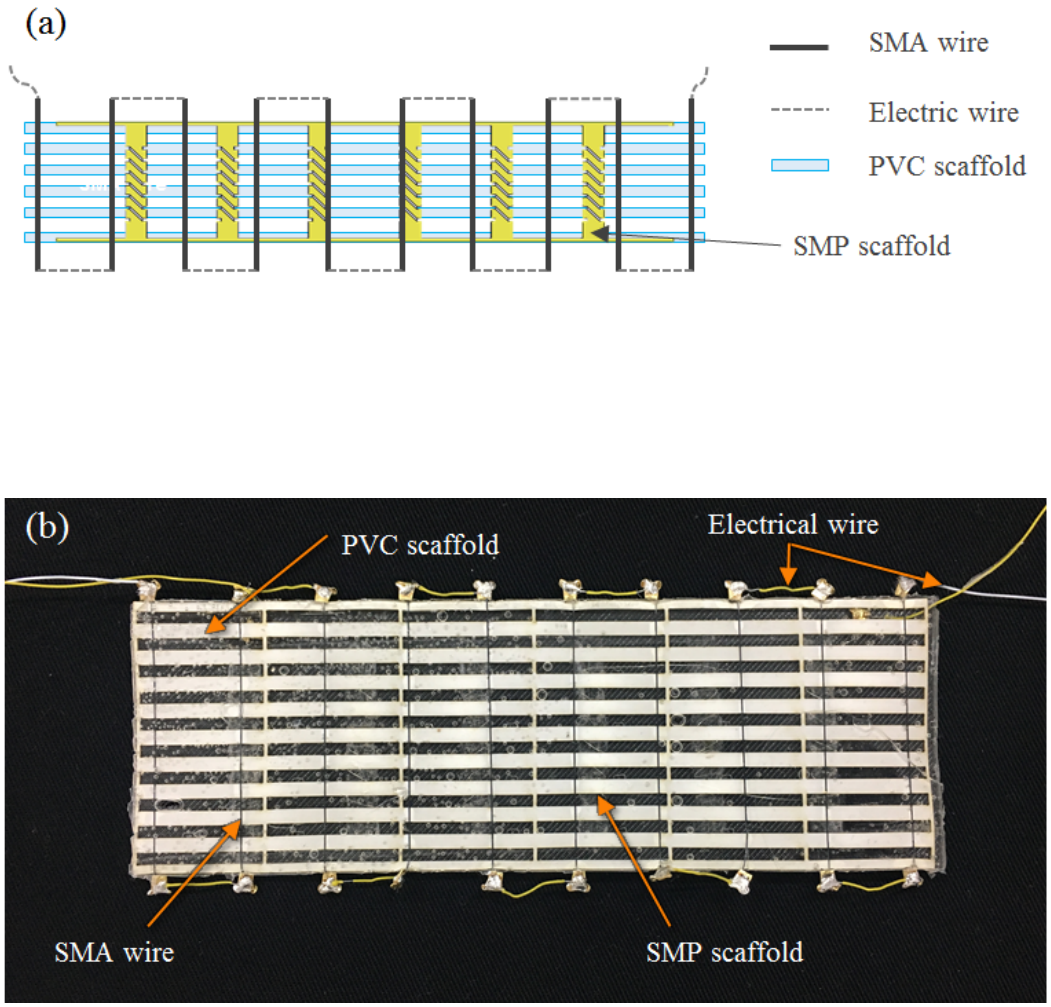

Figure 4.2 (a) Schematic layout of SMP-SMA based composite SSC actuator and (b) fabricated specimen.

4.2 Morphing flap

The fabricated SMP-SMA based SSC actuator was inserted into the flap mold, a computer numerical control(CNC)-machined acrylic mold that had the same inner curvature as the wing. Then, the internal structure was placed to make a surface pattern and set the internal space of the morphing flap. In the assembled mold, PDMS was injected, and the structure was cured at 55℃ for 8 h in an oven. After curing the PDMS, the internal structure was replaced for eco-flex injection. The eco-flex used in this step was Eco-flex 0030 (Smoothon, Inc., with parts A to B mixed in ratio of 1:1). The reassembled mold was cured at 50℃ for 3 hours in an oven. Figure 4.3 shows the fabrication process of the morphing flap. After curing, the mold was disassembled, and the cured flap was removed. Figure 4.4 shows the fabricated morphing flap.

The cured flap and the 3D-printed flexible structure were connected to the unmorphed wing segment structure as shown in figure 4.5.

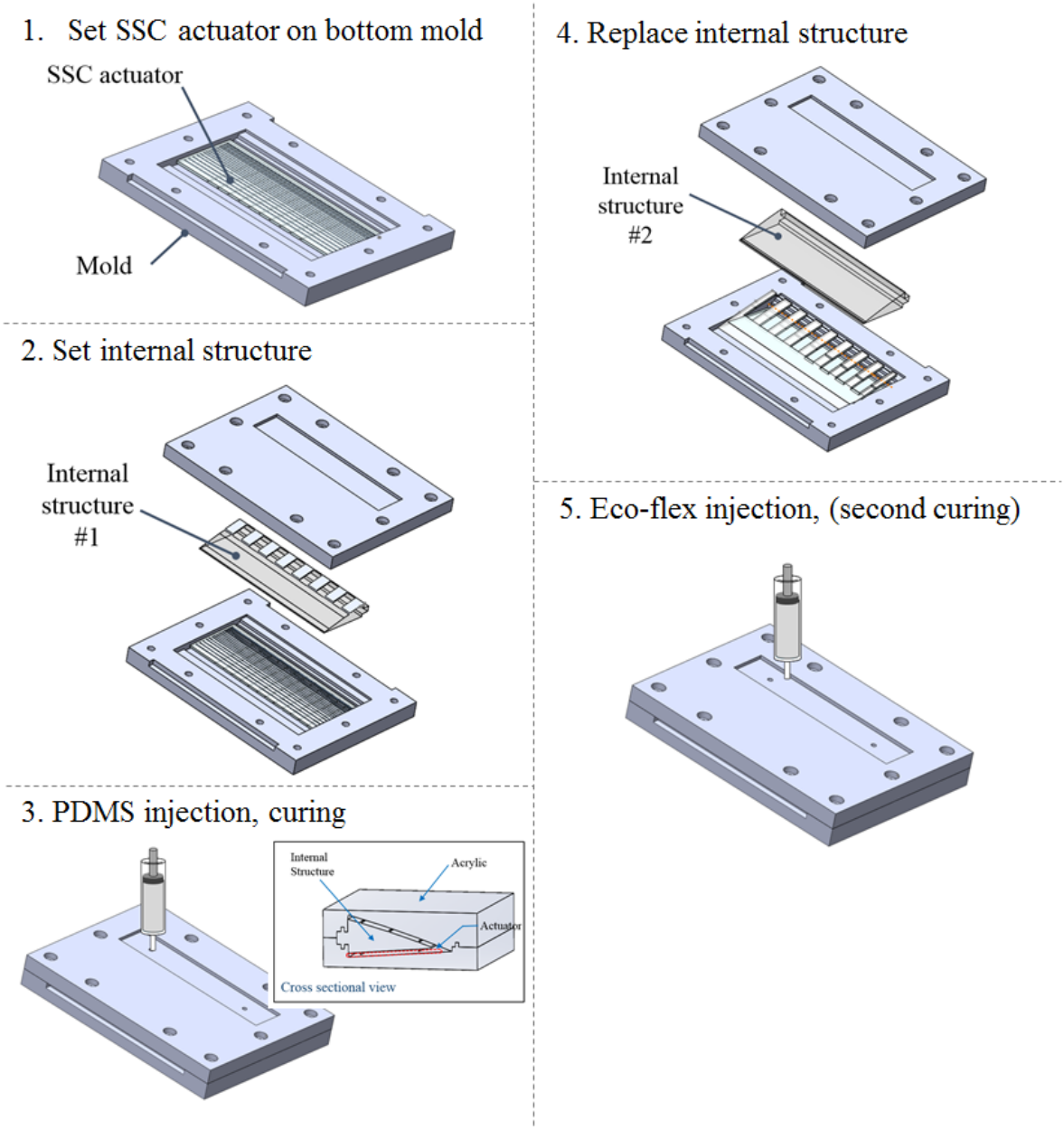

Figure 4.3. The fabrication process for the morphing flap.

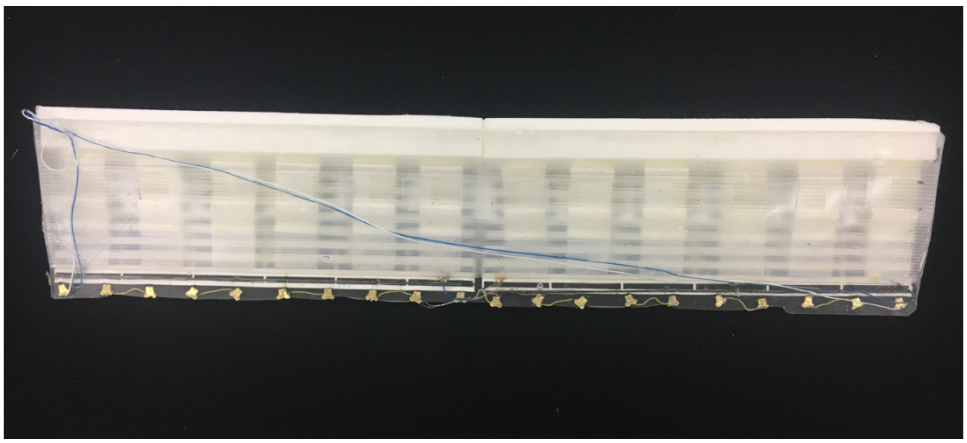

Figure 4.4 Fabricated morphing flap.

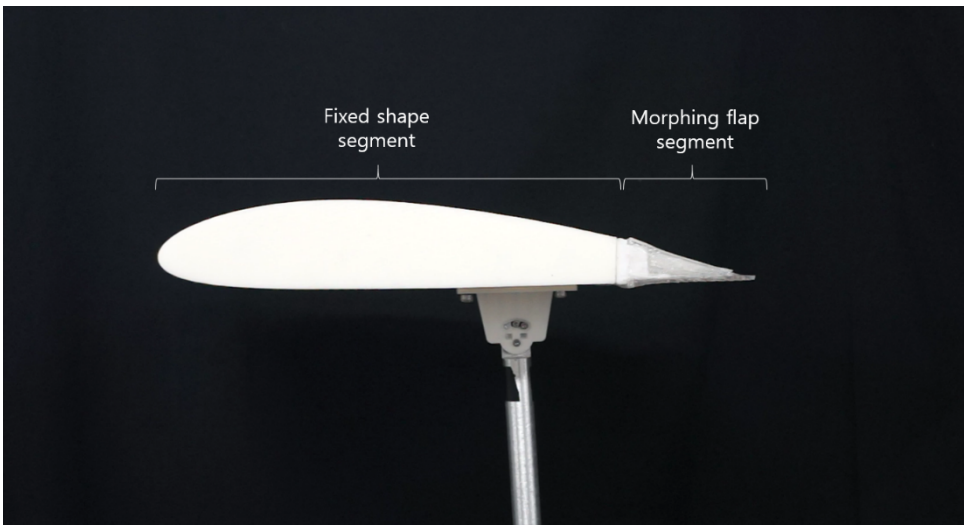

Figure 4.5 Fabricated wing segment with morphing flap.

Chapter 5. Experiment and result

5.1 SMP-SMA based SSC actuator performance evaluation

To evaluate the performance of the SMP-SMA-based SSC actuator, cooling and heating tests and deformation tests were performed. Experiments were carried out by fixing the actuator to a fixture in a room-temperature environment as shown in figure 5.1 and then heating and cooling the SMP and SMA using the current.

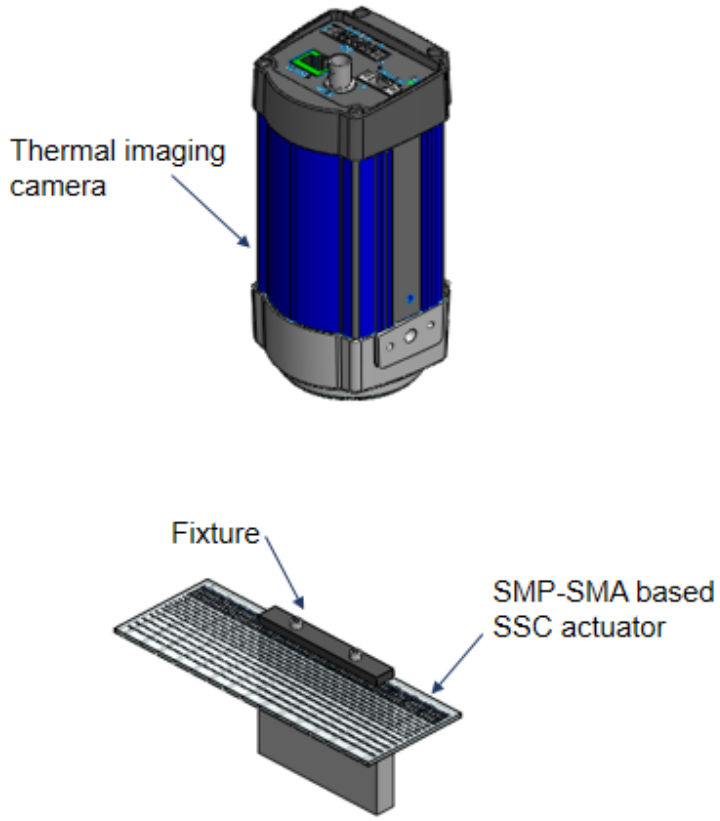

Figure 5.1 Actuator performance experiments set up.

The heating–cooling sequence of the actuator and the temperature changes during actuation are shown in Figure 5.2. To evaluate the heating and cooling performance of the actuator, the temperature changes were observed using a thermal–imaging camera.

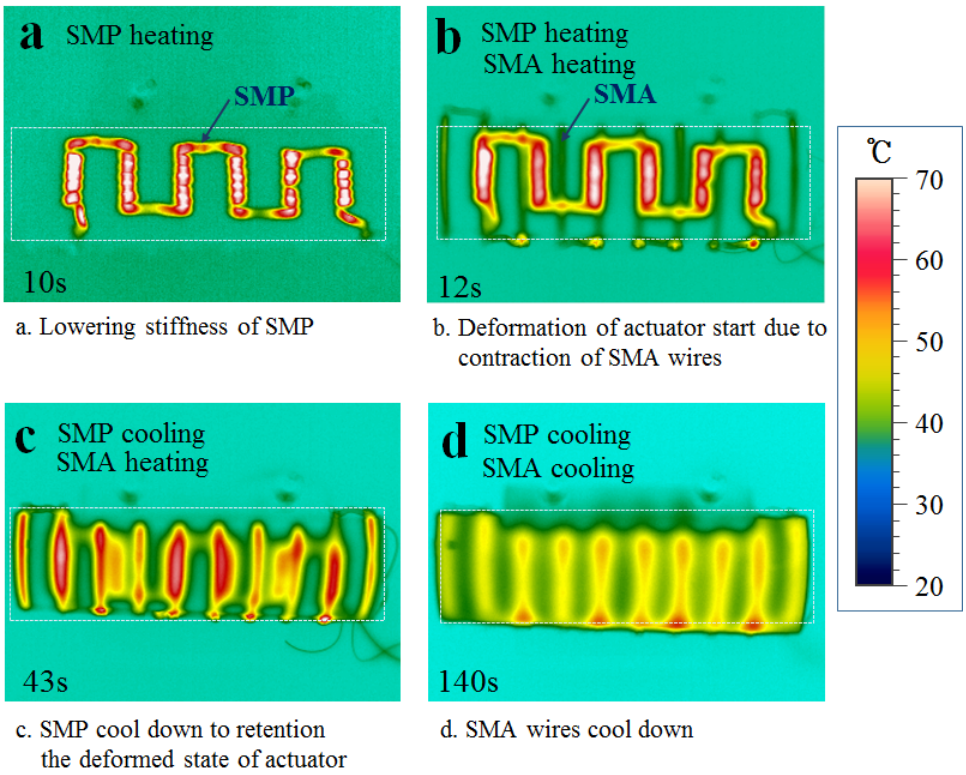

a. Lowering stiffness of SMP

b. Deformation of actuator start due to contraction of SMA wires

c. SMP cool down to retention the deformed state of actuator

d. SMA wires cool down

Figure 5.2. Time-series thermal images of SMP-SMA based actuator surface when each components are heated and cooled.

Figure 5.3 shows that the SMP took 12 s to reach T_g(55℃), using a current of 0.4 A and 180 s to cool down to 30℃ at room temperature.

The bending performance of the actuator can be defined in terms of the maximum deformation angle and the maximum retention angle. The tip deformation angle, the time required to reach the fully deformed state, and the deformation-maintained angle after the SMP scaffold was cooled were measured. The deformation of the actuator according to each actuation sequence is shown in figure 20.

The bending performance was measured by applying a current of 0.7 A to the SMA and a current of 0.4 A to the SMP. When the SMP was in the rubbery state, the maximum deformation angle of the SMA actuator was 101°, and the deformation maintained angle was 70° after cooling the SMP to the glassy state. The deformation-maintained angle of the actuator was reduced by 10° from the maximum deformation angle, due to the elasticity of the PDMS and PVC scaffold.

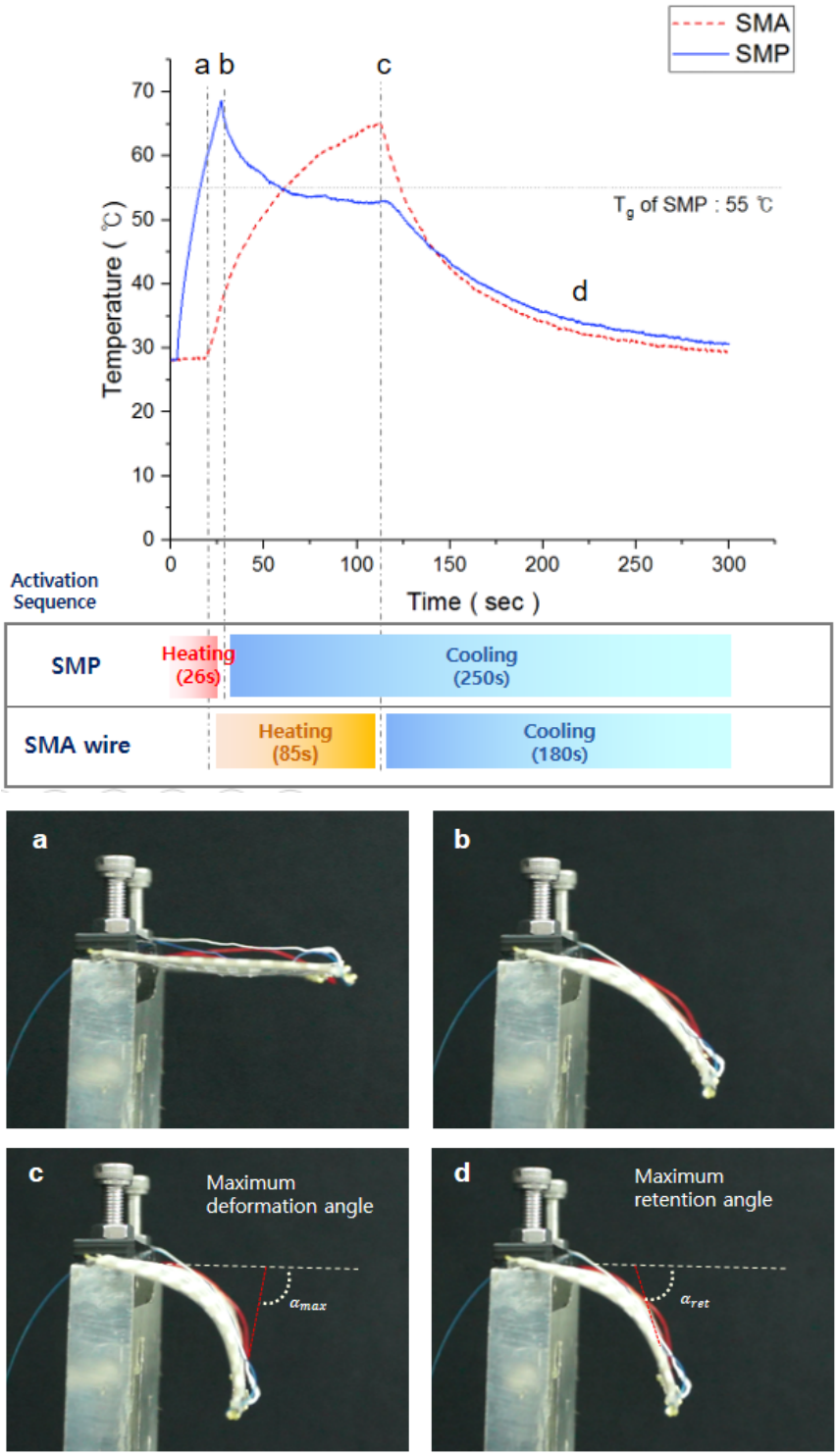

Figure 5.3 Activation sequence, temperature changes, and deformation of SMP and SMA of the SSC.

5.2 Morphing flap performance evaluation

The prototype morphing flap was used to create additional lift force in the wing during specific conditions, such as landing, take-off, and cruising at low speed. We evaluated the performance of the morphing flap with both actuation performance and aerodynamic performance.

The actuation performance of the morphing flap was measured as shown in figure 5.4. The maximum deformation angle was 39° and the retention angle was 32°

The aerodynamic performance of the morphing flap was measured in a closed-type wind tunnel. The load cell for measuring the aerodynamic forces was installed outside the test section of the wind tunnel, and the wing with the morphing flap mounted was placed at the center of the test section using a strut bar as shown in figure 5.5.

The size of the test section was 900 mm × 900 mm and the speed of the wind for the test was 15 m/s, resulting in a Reynolds number of 2.1 × 105, based on the chord length of the wing. The experiment was conducted at room temperature while varying the angle of attack from 2° to 12° at 2° intervals.

To determine the difference between the morphing flap and a conventional flap, a plain, conventional flap with the same chord line was also fabricated and tested. Experiments were carried out with the same angle between flow direction and chord line of the conventional flap and the morphing flap as shown is figure 5.6.

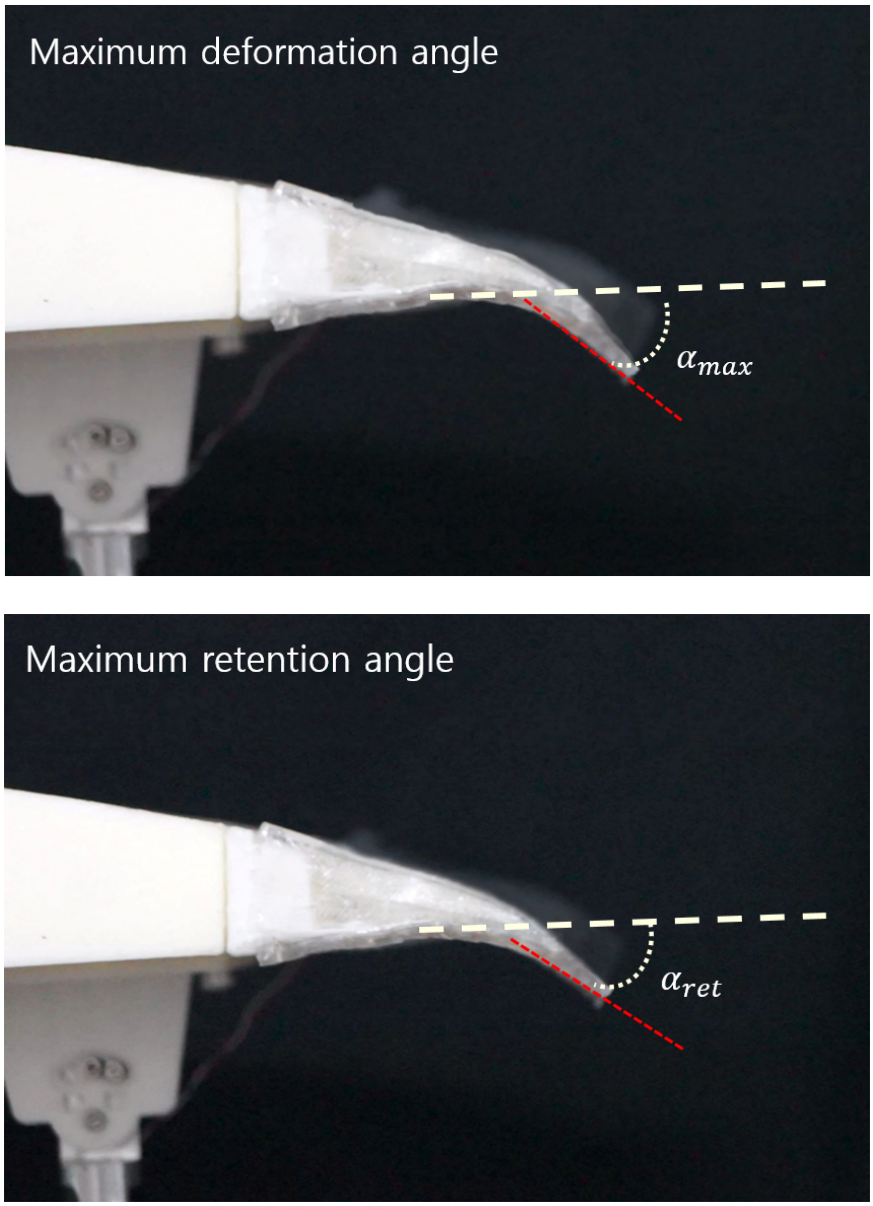

Figure 5.4 Deformation of morphing flap

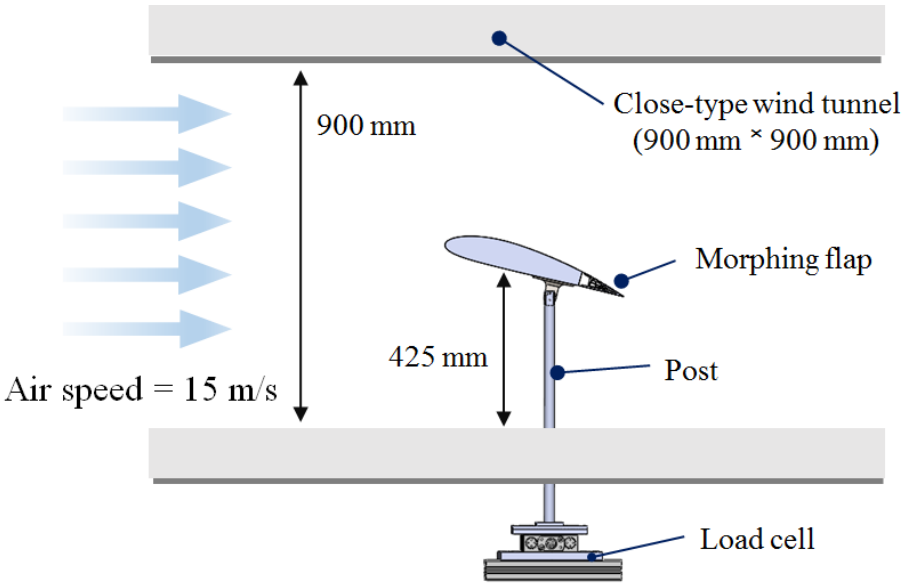

Figure 5.5. The schematic image of wind tunnel experimental set-up

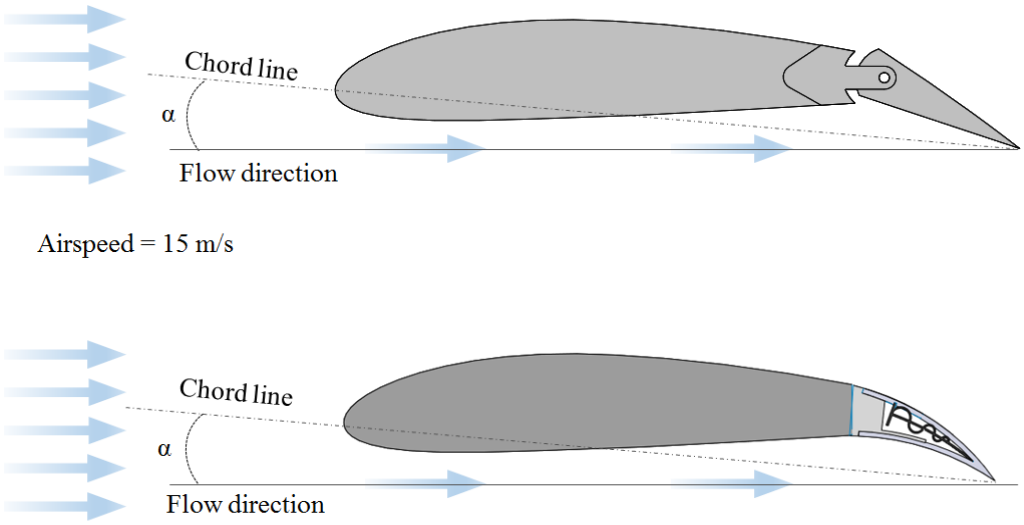

Figure 5.6 The morphing flap and conventional flap experiment set-up

Results for the lift and drag forces of the wing were measured for the unactuated and actuated flap and the conventional flap at different angles of attack (α). As shown in figure 5.7, additional lift occurred when the morphing flap was actuated. The lift coefficient (C_l) and drag coefficient (C_d) can be calculated using Eqs. (1) and (2) :

$$C_l = \frac{L}{\frac{1}{2}\rho v^2 s} \quad (1)$$

$$C_d = \frac{D}{\frac{1}{2}\rho v^2 s} \quad (2)$$

(L: lift force, D : drag force, ρ : mass density of air, v : wind speed s : reference area of the wing)

Figure 5.8 shows the changes in lift and drag coefficient as the angle of attack increases in the unactuated and actuated morphing flap cases. The lift coefficient increased steadily with both the actuated and the unactuated flap as the angle of attack increased. The lift coefficient increased by 27 ~ 50% compared with before flap actuation; the maximum difference was 50% at a 2° angle of attack. The drag coefficient also increased before and after flap actuation as the angle of attack increased. The maximum difference in drag coefficient was 34% at a 2° angle of attack. The difference decreased with an increasing angle of attack.

The lift to drag (L/D) ratio of the morphing flap was calculated from the L/D ratio as shown in figure 5.9. The L/D ratio of the morphing flap showed a tendency to increase with the angle of attack and increased 11~27% when operated. Compared with the conventional flap, the increase was 7~81%; the maximum difference was 81% at a 10° angle of attack.

The maximum L/D ratio with the conventional flap occurred at a 6° angle of attack. The L/D coefficient of the morphing flap improved, compared with the conventional flap, within the experimental range; consequently, the L/D ratio of the morphing flap showed improved aerodynamic performance versus the corresponding conventional flap.

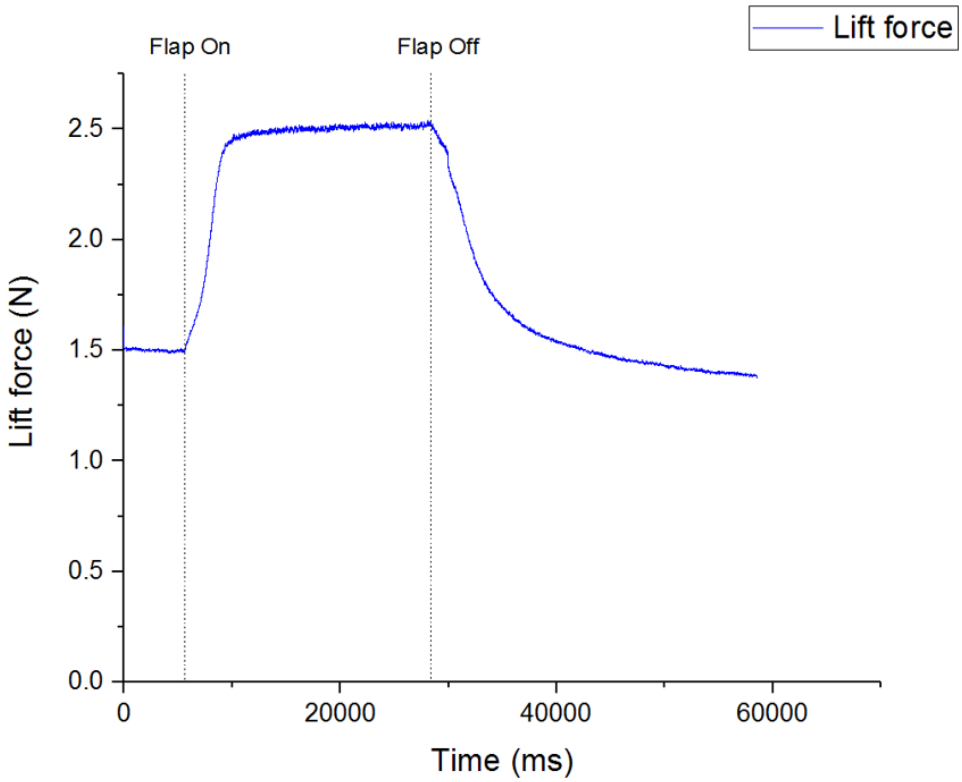

Figure 5.7. Changes in lift forces depend on morphing flap actuation (AOA : 2°)

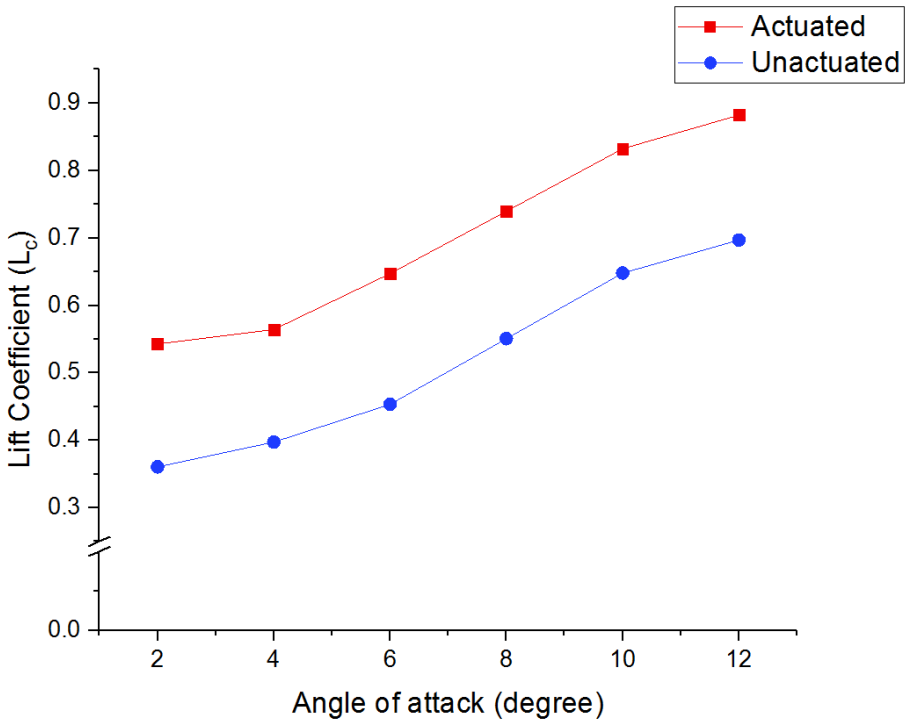

(a) Lift coefficient of the actuated and un-actuated morphing flap

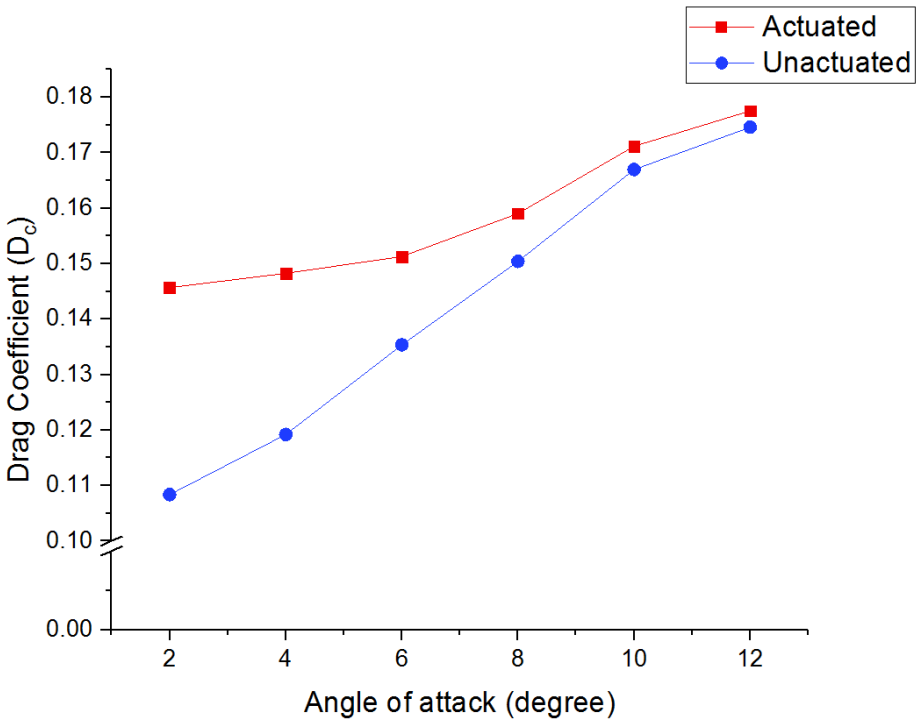

(b) Drag coefficient of the actuated and un-actuated morphing flap

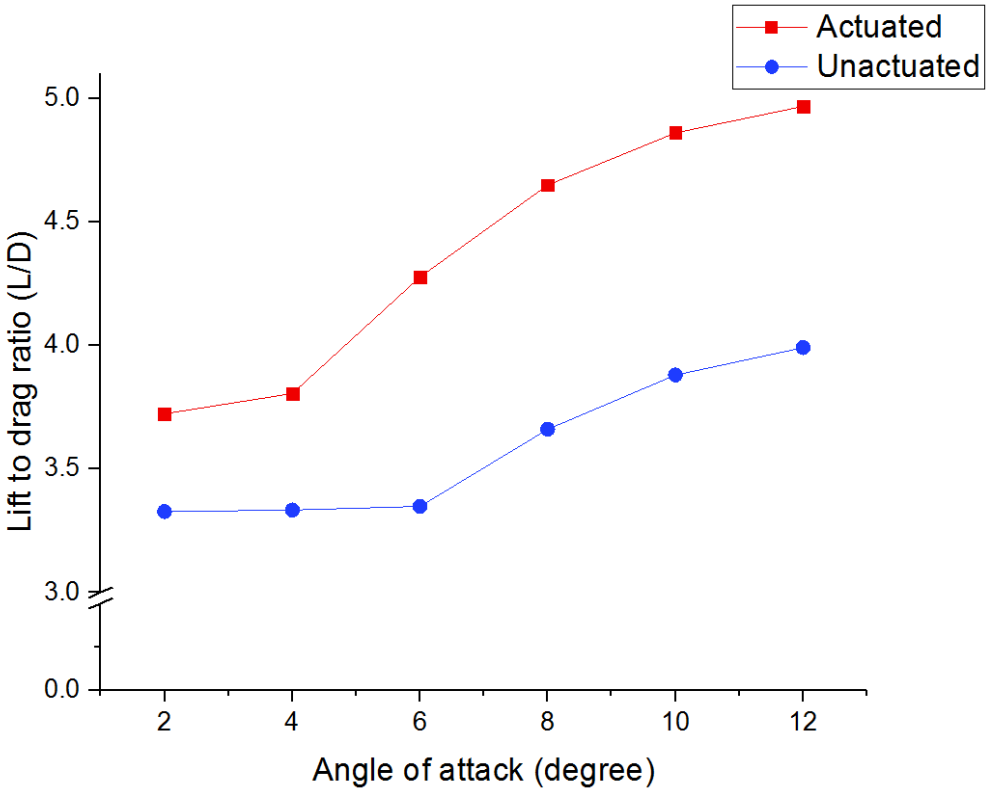

(c) Lift to drag ratio of actuated and un-actuated morphing flap

Figure 5.8 Aerodynamic coefficient of actuated and un-actuated morphing flap as a function of the angle of attack

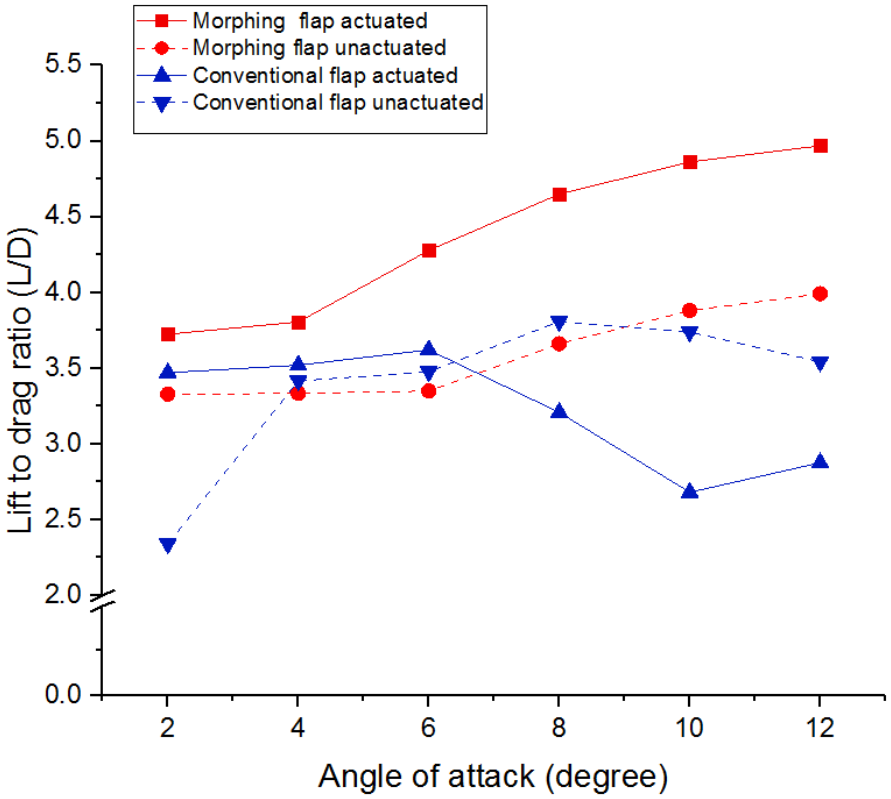

Figure 5.9 Lift to drag ratio of the morphing flap and the conventional flap as a function of the angle of attack

Chapter 6. Conclusion

We designed a SSC actuator using SMP and a SMA wire, and prepared and evaluated the performance of a prototype actuator. Additionally, we designed and fabricated a morphing flap with the SMP-SMA-based SSC actuator and performed wind tunnel experiments with a wing structure of small airplane to assess aerodynamic performance.

The SSC actuator, with a SMA wire and a SMP scaffold integrated into a soft composite, uses the Young's modulus of the SMP in a glassy state to maintain the deformed state after the actuator is deformed. Unlike previous research on developing morphing flaps using smart materials, we developed a morphing flap using SMA and a SMP-based composite actuator, designed as an integrated flap. Improved operation energy efficiency was achieved by controlling the heating and cooling sequences of the SMP and SMA.

The morphing flap fabricated had a continuous surface with the wing; it maintained a smooth and continuous curvature during actuation, improving the aerodynamic performance of the overall wing. The morphing flap also generated additional lift during actuation.

The proposed morphing flap mechanism and design of the morphing flap can be applied to the development of a morphing wing. Thus, we plan to design a morphing wing whereby the entire wing will deform; a custom-designed system will control the flap deformation angle.

Reference

[1] D. C. L. Justin K. Strelec, Mohammad A. Khan and John Yen, "Design and implementation of a shape memory alloy actuated reconfiguration airfoil," *Journal of Intelligent Material Systems and Structures,* vol. 14, pp. 257-273, May 2015 2003.

[2] J. C. Gomez and E. Garcia, "Morphing unmanned aerial vehicles," *Smart Materials and Structures,* vol. 20, no. 10, p. 103001, 2011.

[3] C. Van Dam, "The aerodynamic design of multi-element high-lift systems for transport airplanes," *Progress in Aerospace Sciences,* vol. 38, no. 2, pp. 101-144, 2002.

[4] M. Senthilkumar, "Analysis of SMA actuated plain flap wing," *Journal of Engineering Sience and Technology review,* vol. 5, pp. 39-43, 15 July 2012 2012.

[5] J. Kudva *et al.*, "Design, fabrication, and testing of the DARPA/Wright Lab 'smart wing' wind tunnel model," 1997.

[6] A. D. Young, "The Aerodynamic Characteristics of Flaps," DTIC Document1947.

[7] W.-R. Kang, E.-H. Kim, M.-S. Jeong, I. Lee, and S.-M. Ahn, "Morphing Wing Mechanism Using an SMA Wire Actuator," *International Journal of Aeronautical and Space Sciences,* vol. 13, no. 1, pp. 58-63, 2012.

[8] E. Bone and C. Bolkcom, "Unmanned aerial vehicles: Background and issues for congress," 2003: DTIC Document.

[9] A. Rango *et al.*, "Using unmanned aerial vehicles for rangelands: current applications and future potentials," *Environmental Practice,* vol. 8, no. 03, pp. 159-168, 2006.

[10] C. Zhang and J. M. Kovacs, "The application of small unmanned aerial systems for precision agriculture: a review," *Precision agriculture,* vol. 13, no. 6, pp. 693-712, 2012.

[11] L. A. Haidari *et al.*, "The economic and operational value of using drones to transport vaccines," *Vaccine,* vol. 34, no. 34, pp. 4062-7, Jul 25 2016.

[12] D. Cadogan, W. Graham, and T. Smith, "Inflatable and rigidizable wings for unmanned aerial vehicles," *AIAA paper,* vol. 6630, p. 2003, 2003.

[13] S. Barbarino, O. Bilgen, R. M. Ajaj, M. I. Friswell, and D. J. Inman, "A Review of Morphing Aircraft," *Journal of Intelligent Material Systems and Structures,* vol. 22, no. 9, pp. 823-877, 2011.

[14] A. Y. N. Sofla, S. A. Meguid, K. T. Tan, and W. K. Yeo, "Shape morphing of aircraft wing: Status and challenges," *Materials & Design,* vol. 31, no. 3, pp. 1284-1292, 2010.

[15] J. Blondeau, J. Richeson, and D. J. Pines, "Design, development and testing of a morphing aspect ratio wing using an inflatable telescopic spar," *AIAA paper,* vol. 1718, pp. 7-10, 2003.

[16] Y. Yu, X. Li, W. Zhang, and J. Leng, "Investigation on adaptive wing

structure based on shape memory polymer composite hinge," in *Proc SPIE*, 2007, vol. 6423, pp. 64231D-5.
[17] H. Rodrigue, S. Cho, M.-W. Han, B. Bhandari, J.-E. Shim, and S.-H. Ahn, "Effect of twist morphing wing segment on aerodynamic performance of UAV," *Journal of Mechanical Science and Technology,* vol. 30, no. 1, pp. 229-236, 2016.
[18] M.-W. Han, H. Rodrigue, H.-I. Kim, S.-H. Song, and S.-H. Ahn, "Shape memory alloy/glass fiber woven composite for soft morphing winglets of unmanned aerial vehicles," *Composite Structures,* vol. 140, pp. 202-212, 2016.
[19] J. K. Strelec, D. C. Lagoudas, M. A. Khan, and J. Yen, "Design and implementation of a shape memory alloy actuated reconfigurable airfoil," *Journal of Intelligent Material Systems and Structures,* vol. 14, no. 4-5, pp. 257-273, 2003.
[20] J. L. Pinkerton and R. W. Moses, "A feasibility study to control airfoil shape using THUNDER," 1997.
[21] J. J. Joo, B. Sanders, T. Johnson, and M. I. Frecker, "Optimal actuator location within a morphing wing scissor mechanism configuration," in *Smart Structures and Materials*, 2006, pp. 616603-616603-12: International Society for Optics and Photonics.
[22] S. Bharti, M. Frecker, G. Lesieutre, and J. Browne, "Tendon actuated cellular mechanisms for morphing aircraft wing," in *The 14th International Symposium on: Smart Structures and Materials & Nondestructive Evaluation and Health Monitoring*, 2007, pp. 652307-652307-13: International Society for Optics and Photonics.
[23] A. Y. Sofla, D. M. Elzey, and H. N. Wadley, "An antagonistic flexural unit cell for design of shape morphing structures," in *ASME 2004 International Mechanical Engineering Congress and Exposition*, 2004, pp. 261-269: American Society of Mechanical Engineers.
[24] S. Barbarino, E. I. Saavedra Flores, R. M. Ajaj, I. Dayyani, and M. I. Friswell, "A review on shape memory alloys with applications to morphing aircraft," *Smart Materials and Structures,* vol. 23, no. 6, p. 063001, 2014.
[25] H. Rodrigue, W. Wang, B. Bhandari, M.-W. Han, and S.-H. Ahn, "SMA-based smart soft composite structure capable of multiple modes of actuation," *Composites Part B: Engineering,* vol. 82, pp. 152-158, 2015.
[26] S.-H. Ahn, K.-T. Lee, H.-J. Kim, R. Wu, J.-S. Kim, and S.-H. Song, "Smart soft composite: An integrated 3D soft morphing structure using bend-twist coupling of anisotropic materials," *International Journal of Precision Engineering and Manufacturing,* vol. 13, no. 4, pp. 631-634, 2012.
[27] S.-H. Song, H. Lee, J.-G. Lee, J.-Y. Lee, M. Cho, and S.-H. Ahn, "Design and analysis of a smart soft composite structure for various modes of actuation," *Composites Part B: Engineering,* vol. 95, pp. 155-165, 2016.
[28] J.-E. Shim, Y.-J. Quan, W. Wang, H. Rodrigue, S.-H. Song, and S.-H.

Ahn, "A smart soft actuator using a single shape memory alloy for twisting actuation," *Smart Materials and Structures,* vol. 24, no. 12, p. 125033, 2015.
[29] N. Morgan, "Medical shape memory alloy applications—the market and its products," *Materials Science and Engineering: A,* vol. 378, no. 1, pp. 16-23, 2004.
[30] D. Hartl and D. C. Lagoudas, "Thermomechanical characterization of shape memory alloy materials," in *Shape memory alloys*: Springer, 2008, pp. 53-119.
[31] Z. D. W. M. Huang, C. C. Wang, J. Wei, Y. Zhao, H. Purnawali, "Shape memory materials," *Materials today,* vol. 13, pp. 54-61, 2010.
[32] H.-I. Kim, M.-W. Han, S.-H. Song, and S.-H. Ahn, "Soft morphing hand driven by SMA tendon wire," *Composites Part B: Engineering,* vol. 105, pp. 138-148, 2016.
[33] W.-S. Chu *et al.*, "Review of biomimetic underwater robots using smart actuators," *International Journal of Precision Engineering and Manufacturing,* vol. 13, no. 7, pp. 1281-1292, 2012.
[34] S.-H. Song, J.-Y. Lee, H. Rodrigue, I.-S. Choi, Y. J. Kang, and S.-H. Ahn, "35 Hz shape memory alloy actuator with bending-twisting mode," *Scientific reports,* vol. 6, 2016.
[35] H. Rodrigue, W. Wang, B. Bhandari, M.-W. Han, and S.-H. Ahn, "Cross-shaped twisting structure using SMA-based smart soft composite," *International Journal of Precision Engineering and Manufacturing-Green Technology,* vol. 1, no. 2, pp. 153-156, 2014.
[36] J. Leng, X. Lan, Y. Liu, and S. Du, "Shape-memory polymers and their composites: Stimulus methods and applications," *Progress in Materials Science,* vol. 56, no. 7, pp. 1077-1135, 2011.
[37] D. Ratna and J. Karger-Kocsis, "Recent advances in shape memory polymers and composites: a review," *Journal of Materials Science,* vol. 43, no. 1, pp. 254-269, 2007.
[38] H. Tobushi, S. Hayashi, Y. Sugimoto, and K. Date, "Performance of Shape Memory Composite with SMA and SMP," *Solid State Phenomena,* vol. 154, pp. 65-70, 2009.
[39] P. Ghosh, A. Rao, and A. R. Srinivasa, "Design of multi-state and smart-bias components using Shape Memory Alloy and Shape Memory Polymer composites," *Materials & Design,* vol. 44, pp. 164-171, 2013.
[40] F. Schneider, J. Draheim, R. Kamberger, and U. Wallrabe, "Process and material properties of polydimethylsiloxane (PDMS) for Optical MEMS," *Sensors and Actuators A: Physical,* vol. 151, no. 2, pp. 95-99, 2009.
[41] H.-S. Kim, J.-Y. Lee, W.-S. Chu, and S.-H. Ahn, "Design and Fabrication of Soft Morphing Ray Propulsor: Undulator and Oscillator," *Soft Robotics*.
[42] H. Rodrigue, Wang, W., Han, M.W., Kim J.Y. and Ahn, S.H., ""An overview of Shape Memory Alloy-coupled Actuators and Robots"," *Soft Robotics,* vol. accepted, 2016.

[43] H.-J. Kim, S.-H. Song, and S.-H. Ahn, "A turtle-like swimming robot using a smart soft composite (SSC) structure," *Smart Materials and Structures,* vol. 22, no. 1, p. 014007, 2012.
[44] M.-W. Han *et al.*, "Woven type smart soft composite for soft morphing car spoiler," *Composites Part B: Engineering,* vol. 86, pp. 285-298, 2016.
[45] W. Wang, H. Rodrigue, and S.-H. Ahn, "Smart soft composite actuator with shape retention capability using embedded fusible alloy structures," *Composites Part B: Engineering,* vol. 78, pp. 507-514, 2015.

초록

지능형 연성 복합재 구동기를 이용한 모핑플랩 개발

김남극
기계항공공학부
서울대학교 대학원

모핑플랩은 날개의 트레일링 엣지를 변화시켜 플랩과 같은 역할을 수행할 수 있다. 모핑플랩의 장점은 날개의 형상을 연속적으로 유지하여 기존의 플랩이 날개와 플랩사이의 불연속적인 형상으로 인해 발생하는 난류나 공기역학적 항력, 진동, 소음과 같은 요소를 저감할 수 있다는것이다. 지능형재료를 이용한 모핑기술은 모터나 유압장치, 힌지와 같은 기계장치를 필요로하지 않고 생체모방 로봇이나 항공분야 등 다양한 분야에 적용이 가능하다. 모핑기술의 이러한 특성은 항공기의 중량을 감소할 수 있기 때문에 항공기 운영비용의 절감할 수 있는 장점으로 작용한다.

이 연구에서는 형상기억폴리머 구조체와 형상기억합금 와이어가 결합된 지능형 연성 복합재 구동기를 설계 및 제작할 것이다. 또한 제작된 형상기억폴리머-형상기억합금 기반 지능형 연성 복합재 구동기는 형상기억합금 와이어에 지속적으로 전류를 가하지 않아도 변형된 상태를 유지할 수 있으며, 최대 변형각도는 102° 그리고 최대 변형 유지각도는 70°의 성능을 가졌다.

모핑플랩은 형상기억폴리머-형상기억합금 기반 지능형 연성 복합재 구동기를 이용하여 제작되었으며, 풍동실험을 통해 공기역학적 성능을

평가하였다. 모핑플랩은 기존의 전통적인 플랩에 비해 양항비가 향상되었으며, 받음각 10°에서 최대 81% 향상된 성능을 보였다.

Keyword : 지능형 재료 ; 모핑구조 ; 모핑플랩 ; 지능형 연성 복합재

Student Number : 2015-20711